Available at
http://pvamu.edu/aam
Appl. Appl. Math.
ISSN: 1932-9466

Applications and
Applied Mathematics:
An International Journal
(AAM)

Special Issue No. 2 (May 2016), pp. 37 – 51
18th International Mathematics Conference, March 20 – 22, 2014, IUB Campus, Bashundhara
Dhaka, Bangladesh

Spectral Numerical Calculation of Non-isothermal Flow through a Rotating Curved Rectangular Duct with Moderate Curvature

Md. Zohurul Islam[1*], Md. Saidul Islam[2] and Rabindra Nath Mondal[3]

[1]Department of Mathematics and Statistics
Jessore University of Science and Technology
Jessore-7408, Bangladesh
[2]Department of Mathematics
Faculty of Science, Engineering and Technology
Hamdard University
New Town, Narayangong, Bangladesh
[3]Department of Mathematics
Jagannath University
Dhaka-1100, Bangladesh
[*]Email: zohurulmathku@gmail.com

ABSTRACT

The present paper investigates non-isothermal flow characteristics through a rotating curved rectangular duct, where co-existence of the rotational forces and fluid temperature gradients leads to the emergence of rotation-induced buoyancy effects. A spectral-based numerical scheme is employed as the principal tool for the simulation while Chebyshev polynomial and collocation method as the secondary tools. The outer wall of the duct is heated while the inner wall cooled, the top and bottom walls being thermally insulated. The emerging parameters controlling the flow characteristics are the rotation parameter, i.e., the Taylor number *Tr* ranging 0 to 2000, the Grashof number *Gr* = 100, the Prandtl number *Pr*, the aspect ratio, and the pressure-driven parameter, i.e., the Dean number *Dn* between 100 and 1000. The flow structures are examined under combined action of the centrifugal, Coriolis and buoyancy forces. As a result, asymmetric 2-cell structures are computed for small values of *Tr* while asymmetric 6-cell structures for large *Tr*. Unsteady flow characteristics show that the flow undergoes in the scenario '*chaotic*→ *multi-periodic* → *periodic*→ *steady-state*', if *Tr* is increased in the positive direction. Typical contours of secondary flow patterns, temperature profiles and axial flow distribution are also obtained at several values of *Tr*, and it is found that there exist asymmetric two- to multi-vortex solutions. Heating the outer wall is found to generate a significant temperature gradient at the outer concave wall.

KEYWORDS: Curved rectangular duct; Dean number; Taylor number and time evolution

AMS-MSC 2010 No.: 76U05, 76E06

1. INTRODUCTION

Rotating flow is an important branch of fluid dynamics and is full of complex physics. In practical applications, rotating thermal flows occur frequently in a variety of rotating machinery. For a long time this intriguing branch of thermal flows has attracted much attention of the researchers. In the past decades, there have appeared several books and review articles on hydrodynamic and heat transfer characteristics of rotating flows. Since rotating machines were introduced into engineering applications, such as rotating systems, gas turbines, electric generators, heat exchangers, cooling system and some separation processes, scientists have paid considerable attention to study rotating curved duct flows. The readers are referred to Nandakumar and Masliyah (1986), Ito (1987) and Yanase et al. (2002) for some outstanding reviews on curved duct flows. The fluid flow in a rotating curved duct is subjected to two forces: the *Coriolis force* due to rotation and the *centrifugal force* due to curvature of the duct. For isothermal flows of a constant property fluid, the Coriolis force tends to produce vortices while centrifugal force is purely hydrostatic. In a curved passage, centrifugal forces are developed in the flow due to channel curvature causing a counter rotating vortex motion applied on the axial flow through the curved channel by Zohurul et al. (2014). This creates characteristics spiraling fluid flow in the curved passage known as secondary flow. At a certain critical flow condition and beyond, additional pairs of counter rotating vortices appear on the outer concave wall of curved fluid passages. This flow condition is referred to as Dean's *hydrodynamic instability* and the additional vortices are known as *Dean Vortices*, in recognition of the pioneering work in this field by Dean (1927).

When a temperature field is applied to the fluid then the variation of fluid density occurs in non-isothermal flows, both Coriolis and centrifugal type buoyancy forces can contribute to the generation of vortices referred Mondal et al. (2007). These two effects of rotation either enhance or counteract each other in a non-linear manner depending on the direction of wall heat flux and the flow domain. Therefore, the effect of system rotation is more subtle and complicated and yields new; richer features of flow and heat transfer in general, bifurcation and stability in particular, for non-isothermal flows. However, analytical, numerical and experimental investigations, such as Baylis (1971), Mondal et al. (2014) and Humphrey et al. (1977) concluded that Dean number was solely responsible for generating secondary flow and Dean instability in curved passages. Mondal et al. (2014) applied an spectral-based numerical study to investigate combined effects of centrifugal and Coriolis instability of the flow through a rotating curved rectangular duct of small curvature, where they investigated unsteady flow characteristics for small values of the flow parameters with positive rotation of the duct, and presented some preliminary results of the flow evolution. Selmi et al. (1994) examined combined effects of system rotation and curvature on the bifurcation structure of two-dimensional flows in a rotating curved duct with square cross section. Wang and Cheng (1996), employing finite volume method, examined the flow characteristics and heat transfer in curved square ducts for positive rotation and found reverse secondary flow for the co-rotation cases. Selmi and Nandakumer (1999) and Yamamoto et al. (1999) performed studies on the flow in a rotating curved rectangular duct. Norouzi et al. (2010) investigated on the inertial and creeping flow of a second-order fluid in a curved duct with square cross-section by using finite difference method.

The effect of centrifugal force due to the curvature of the duct and the opposing effects of the first and second normal stress difference on the flow field were investigated in that study. Chandratilleke et al. (2012) presented extensive 3D computational study using helicity function that describes the secondary vortex structure and thermal behavior in the fluid flow

through curved rectangular ducts of aspect ratios ranging from 1 to 6. A curvilinear coordinate system was used in that study facilitating effective grid definition for capturing vortex generation and permitting efficient evaluation of local pressure gradient. Norouzi and Biglari (2013) performed, for the first time, an analytical solution of Dean Flow inside a curved rectangular duct, where perturbation method was used to solve the governing equations. The main flow velocity (axial flow), vector plots of lateral velocity (secondary flows) and flow resistance ratios were obtained in that study. Their study was limited to low Reynolds numbers and obtained maximum four-vortex solutions. Wu et al. (2013) performed numerical study of the secondary flow characteristics in a curved square duct by using the spectral method, where the walls of the duct except the outer wall rotate around the Centre of curvature and an azimuthally pressure gradient was imposed. In that study, multiple solutions with 2-vortex, 4-vortex, 8-vortex and even non-symmetric vortices were obtained at the same flow condition.

Recently, Kun et al. (2014) performed an experimental investigation on laminar flows of pseudo-plastic fluids in a square duct of strong curvature using an ultrasonic Doppler velocimetry and microphones, where stream wise velocity in the cross-section of the duct and the fluctuating pressure on the walls were measured for different flow rates. Guo et al. (2011) used a laminar incompressible three- dimensional numerical model to explore the interactive effects of geometrical and flow characteristics on heat transfer and pressure drop. They applied entropy generation as a hydro-thermal criterion and reported the influence of the Reynolds number and curvature ratio on the flow profile and the Nusselt number. Recently, Mondal et al. (2012, 2013a, 2013b) performed numerical investigation on the non-isothermal flow through a rotating curved square and rectangular duct and obtained substantial results. To the best of the authors' knowledge, however, there has not yet been done detail investigation on the unsteady flow characteristics for the non-isothermal flow through a curved rectangular duct of moderate aspect ratio with pressure gradient in the axial direction. But from the scientific as well as engineering point of view it is quite interesting to study the unsteady flow behavior in the presence of strong centrifugal and buoyancy forces for moderate aspect ratio of the duct, because this type of flow is often encountered in engineering applications such as in gas turbines, metallic industry and exhaustive pipes. The present paper investigates unsteady flow characteristics for the non-isothermal flow through a rotating curved rectangular duct by using the spectral method, and covering a wide range of the Dean number and the Taylor number. Studying the effects of system rotation on the flow characteristics, caused by the centrifugal-Coliolis-buoyancy forces with pressure drop, is an important objective of the present study.

2. PHYSICAL MODEL

Consider fully developed two-dimensional flow of viscous incompressible fluid through a rotating curved rectangular duct whose height and width are *2h* and *2d*, respectively. The coordinate system with the relevant notation is shown in Figure 1, where *x′* and *y′* axes are taken to be in the horizontal and vertical directions respectively, and *z'* is the axial direction of the duct. The system rotates at a constant angular velocity Ω_T and the representative velocity $U_0 = \frac{\nu}{d}$, where ν is the kinematic viscosity. We introduce the non-dimensional variables defined as:

$$u=\frac{u'}{U_0},\quad v=\frac{v'}{U_0},\quad w=\frac{\sqrt{2\delta}}{U_o}w',\ x=\frac{x'}{d},\quad y=\frac{y'}{d},\quad z=\frac{z'}{d},\ T=\frac{T'}{\Delta T'},\quad t=\frac{U_0}{d}t',$$
$$\delta=\frac{d}{L},\ P=\frac{P'}{\rho\ U_0^{\ 2}},\ G=\ -\frac{\partial P'}{\partial\ z'}\frac{d}{\rho U_0^2},$$

where *u*, *v*, and *w* are the non-dimensional velocity components in the *x*, *y* and *z* directions, respectively; *t* is the non-dimensional time, *P* the non-dimensional pressure, δ the non-dimensional curvature, and temperature is non-dimensionalized by ΔT. Henceforth, all the variables are non-dimensionalized if not specified.

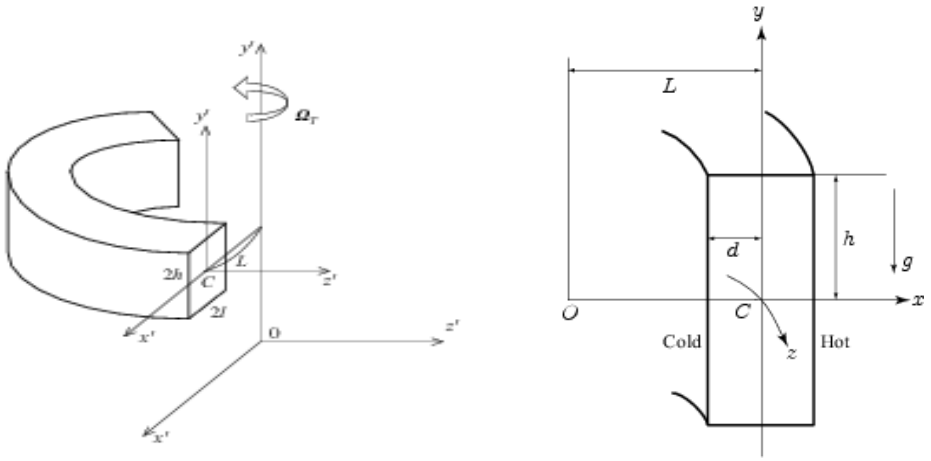

Figure 1. Physical configuration of the system

3. MATHEMATICAL FORMULATION

Since the flow field is uniform in the z-direction, the sectional stream function ψ is introduced as,

$$u=\frac{1}{1+\delta x}\frac{\partial\psi}{\partial y},\quad v=-\frac{1}{1+\delta x}\frac{\partial\psi}{\partial x}. \tag{1}$$

A new coordinate variable *y* is introduced in the y' direction as $y=ay'$, where $a=h/d$ is the aspect ratio of the duct cross section. From now on y denotes y' for the sake of simplicity. Then the basic equations for the axial velocity w, the stream function ψ and the temperature T are derived from the Navier-Stokes equations and the energy equation under the *Boussinesq approximation* as,

$$(1+\delta x)\frac{\partial w}{\partial t}+\frac{1}{a}\frac{\partial(w,\psi)}{\partial(x,y)}-Dn+\frac{\delta^2 w}{1+\delta x}=(1+\delta x)\Delta_2 w-\frac{1}{a}\frac{\delta}{(1+\delta x)}\frac{\partial\psi}{\partial y}w+\delta\frac{\partial w}{\partial x}-\delta Tr\frac{\partial\psi}{\partial y}, \tag{2}$$

$$\left(\Delta_2-\frac{\delta}{1+\delta x}\frac{\partial}{\partial x}\right)\frac{\partial\psi}{\partial t}=-\frac{1}{a}\frac{1}{(1+\delta x)}\frac{\partial(\Delta_2\psi,\psi)}{\partial(x,y)}+\frac{1}{a}\frac{\delta}{(1+\delta x)^2}\times\left[\frac{\partial\psi}{\partial y}\left(2\Delta_2\psi-\frac{3\delta}{1+\delta x}\frac{\partial\psi}{\partial x}+\frac{\partial^2\psi}{\partial x^2}\right)\right.$$

$$-\frac{\partial\psi}{\partial x}\frac{\partial^2\psi}{\partial x\partial y}\Bigg]+\frac{\delta}{(1+\delta x)^2}\times\left[3\delta\frac{\delta^2\psi}{\partial x^2}-\frac{3\delta^2}{1+\delta x}\frac{\partial\psi}{\partial x}\right]-\frac{2\delta}{1+\delta x}\frac{\partial}{\partial x}\Delta_2\psi+\frac{1}{a}w\frac{\partial w}{\partial y}+\Delta_2^2\psi$$

$$-Gr(1+\delta x)\frac{\partial T}{\partial x}-\frac{1}{2}Tr\frac{\partial w}{\partial y}, \tag{3}$$

$$\frac{\partial T}{\partial t}+\frac{1}{(1+\delta x)}\frac{\partial(T,\psi)}{\partial(x,y)}=\frac{1}{\Pr}\left(\Delta_2 T+\frac{\delta}{1+\delta x}\frac{\partial T}{\partial x}\right), \tag{4}$$

where

$$\Delta_2\equiv\frac{\partial^2}{\partial x^2}+\frac{1}{a^2}\frac{\partial^2}{\partial y^2},\quad\frac{\partial(f,g)}{\partial(x,y)}\equiv\frac{\partial f}{\partial x}\frac{\partial g}{\partial y}-\frac{\partial f}{\partial y}\frac{\partial g}{\partial x}.$$

The non-dimensional parameters Dn, the Dean number; Tr, the Taylor number; Gr, the Grashof number and Pr, the prandtl number, which appear in equations (2) to (4) are defined as:

$$Dn=\frac{Gd^3}{\mu\upsilon}\sqrt{\frac{2d}{L}},\quad Tr=\frac{2\sqrt{2\delta}\Omega_T d^3}{\upsilon\delta},\ Gr=\frac{\beta g\Delta T d^3}{\upsilon^2},\quad \Pr=\frac{\upsilon}{\kappa}, \tag{5}$$

where μ, β, κ and g are the viscosity, the coefficient of thermal expansion, the co-efficient of thermal diffusivity and the gravitational acceleration respectively, υ is the viscosity of the fluid. In the present study, Dn and Tr are varied while Gr, a, δ and Pr are fixed. The physical properties with various parameters used in the present study, are shown in Table 1.0

Table 1. Parameters with physical properties

Parameters	**Physical properties**	**Present Values**
Dean number (Dn)	Pressure gradient	$100 \le Dn \le 1000$
Taylor number (Tr)	Non-dimensional rotational parameter	$0 \le Tr \le 2000$
Grashof number (Gr)	Dimensionless natural convection parameter that governs the fluid flow	$Gr = 100$
Aspect ratio (a)	-	a = 2.0
Curvature (δ)	-	$\delta = 0.1$
Prandtl number (Pr)	Characteristic of the fluid	Pr = 7.0 (water)

4. BOUNDARY CONDITIONS

The boundary conditions for w and ψ of the present study are described as follows:

$$w(\pm1,y)=w(x,\pm1)=\psi(\pm1,y)=\psi(x,\pm1)=\frac{\partial\psi}{\partial x}(\pm1,y)=\frac{\partial\psi}{\partial y}(x,\pm1)=0. \tag{6}$$

Also, the temperature T is constant on the walls as

$$T(1, y) = 1, \quad T(-1, y) = -1, \quad T(x, \pm 1) = x. \tag{7}$$

5. Numerical methods

5.1. Method of numerical calculations

In order to solve the system of non-linear partial differential equations (2) to (4) numerically, the spectral method is used. By this method the expansion functions $\phi_n(x)$ and $\psi_n(x)$ are expressed as,

$$\left.\begin{aligned} \varphi_n(x) &= (1-x^2)\,C_n(x), \\ \psi_n(x) &= (1-x^2)^2 C_n(x) \end{aligned}\right\}, \tag{8}$$

where $C_n(x) = \cos\left(n\cos^{-1}(x)\right)$ is the n^{th} order Chebyshev polynomial. $w(x, y, t)$, $\psi(x, y, t)$ and $T(x, y, t)$ are expanded in terms of the expansion functions $\phi_n(x)$ and $\psi_n(x)$ as

$$\left.\begin{aligned} w(x,y,t) &= \sum_{m=0}^{M}\sum_{n=0}^{N} w_{mn}(t)\,\phi_m(x)\,\phi_n(y) \\ \psi(x,y,t) &= \sum_{m=0}^{M}\sum_{n=0}^{N} \psi_{mn}(t)\,\psi_m(x)\,\psi_n(y) \\ T(x,y,t) &= \sum_{m=0}^{M}\sum_{n=0}^{N} T_{mn}\,\phi_m(x)\,\phi_n(y) + x \end{aligned}\right\}, \tag{9}$$

where M and N are the truncation numbers along x and y directions respectively. We performed graphical representation of the time-evolution of the unsteady solutions, secondary flow behavior, temperature profiles and axial flow distribution. As a result, multiple solutions of steady-state, periodic, multi-periodic and chaotic solutions with symmetric and asymmetric multi-vortex solutions are obtained.

5.2. Grid sensitivity test

The accuracy of the numerical calculations is investigated for the truncation numbers M and N used in this study. Five types of grid sizes were used to check the dependence of grid size (i.e., M and N). For good accuracy of the solutions, N is chosen equal to $2M$. Different types of the grid sizes are taken in this study as $14\times 28,\ 16\times 32, 18\times 36, 20\times 40, 22\times 44$, and it is found that M = 16 and N = 32 gives sufficient accuracy of the numerical solutions, which are shown in Table 2.

Table 2. The values of λ and $w(0,0)$ for various *M* and *N* at $Dn = 700$ and $Tr = 830$

M	*N*	λ	$w(0,0)$
14	28	0.3396734	185.2898
16	**32**	**0.3396702**	**185.4422**
18	36	0.33960845	185.5519
20	40	0.33965815	185.6331

In order to calculate the unsteady solutions, Crank-Nicolson and Adams-Bashforth methods together with the function expansion (9) and the collocation methods are applied. Details of these methods are discussed in Mondal (2006). By applying the Crank- Nicolson and the Adams-Bashforth methods to the non-dimensional basic equations (2)-(4), and rearranging, we get

$$\left(\frac{1}{\Delta t}-\frac{\Delta_2}{2}\right)w(t+\Delta t)=\left(\frac{1}{\Delta t}+\frac{\Delta_2}{2}\right)w(t)-\delta x\frac{w(t)-w(t-\Delta t)}{\Delta t}+P(x,\ y). \tag{10}$$

$$\left(\frac{1}{\Delta t}-\frac{\Delta_2}{2}\right)\Delta_2\psi(t+\Delta t)=\left(\frac{1}{\Delta t}+\frac{\Delta_2}{2}\right)\Delta_2\psi(t)+\frac{\delta}{1+\delta x}\frac{1}{\Delta t}\left(\frac{\partial\psi(t)}{\partial x}-\frac{\partial\psi(t-\Delta t)}{\partial x}\right)+Q(x,\ y). \tag{11}$$

$$\left(\frac{1}{\Delta t}-\frac{\Delta_2}{2\,\mathrm{Pr}}\right)T(t+\Delta t)=\left(\frac{1}{\Delta t}+\frac{\Delta_2}{2\,\mathrm{Pr}}\right)T(t)+R(x,\ y). \tag{12}$$

In the above formulations, P, Q and R are the non-linear terms. Then applying the Adams-Bashforth method for the second term of R. H. S of Equations (10), (11) and (12) and simplifying we calculate $w(t+\Delta t)$, $\psi(t+\Delta t)$ and $T(t+\Delta t)$ by numerical computation.

5.3. Resistance coefficient

We use the resistance coefficient λ as one of the representative quantities of the flow state. It is also called the *hydraulic resistance coefficient* and is generally used in fluids engineering defined as,

$$\frac{P_1^*-P_2^*}{\Delta z^*}=\frac{\lambda}{dh^*}\frac{1}{2}\rho\left\langle w^*\right\rangle^2, \tag{13}$$

where quantities with an asterisk denote the dimensional ones, $\langle\rangle$ stands for the mean over the cross section of the rectangular duct, and $d_h^*=4(2d\times 4dh)/(4d\times 8dh)$. Since $\left(P_1^*-P_2^*\right)/\Delta z^*=G$, λ is related to the mean non-dimensional axial velocity $\langle w\rangle$ as

$$\lambda=\frac{16\sqrt{2\delta}Dn}{3\langle w\rangle^2}, \tag{14}$$

Where

$$\langle w\rangle=\sqrt{2\delta}d/\nu\left\langle w^*\right\rangle.$$

In this paper, λ is used to calculate the unsteady solutions by numerical computations.

6. Results and Discussion

In the present model, our objective is to study the effects of rotation on the flow characteristics. The expressions for velocity profile, flow rate, wall heat transfer (temperature profile) are obtained by solving the governing equation of flow using the spectral method. In this paper, time evolution calculations of the resistant coefficient λ are performed for the non-isothermal flows over a wide range of the Dean Numbers (Dn) and the Taylor Number (Tr) for the two cases of the duct rotation, *Case I*: Dn = 700 and *Case II*: Dn = 1000.

6.1. *Case I*: Dean Number, Dn = 700

We performed time evolution of λ for $0 \leq Tr \leq 2000$ and $100 \leq Dn \leq 1000$. Figure 2(a) shows time evolution of λ for Tr = 100 and Dn = 700 at Gr = 100. It is found that the unsteady flow at Tr = 100 is a chaotic solution which is well justified by drawing the phase spaces as shown in Figure 2(b). Figure 2(c) shows typical contours of secondary flow patterns, temperature profiles and axial flow distribution for Tr = 100 and Dn = 700, where we find that the unsteady flow is a four-vortex solution. This is caused by the combined action of the Coriolis force and centrifugal force by Wang and Cheng (1996). Then we performed time evolution for Tr = 800 as shown in Figure 3(a). It is found that the unsteady flow at Tr =800 is a weak chaotic solution which is transformed into the multi-periodic solution, and it is well justified by drawing the phase spaces as shown in Figure 3(b). Contours of secondary flow patterns, temperature profiles and axial flow distribution for the corresponding flow patterns are shown in Figure 3(c), where it is found that the multi-periodic oscillation at Tr = 800 is a four-vortex solution. The time evolution for Tr = 830 is shown in Figure 4(a). It is found that the unsteady flow at Tr =830 is a fully multi-periodic solution whose orbit is different and it is well justified by drawing the phase space as shown in Figure 4(b). Contours of secondary flow patterns, temperature profiles and axial flow distribution for the corresponding flow patterns are shown in Figure 4(c), where it is found that the multi-periodic oscillation at Tr = 830 is a four-vortex solution.

In this paper, the buoyancy effects caused by the differentially heated vertical sidewalls are clearly shown. The buoyancy effects are due to the centrifugal and Coriolis forces in the presence of a density gradient. When a duct is rotated, heating or cooling of the fluid which is contained in or flow through it, can give rise to significant buoyant force effects. The present work, therefore, confines itself to the thermal buoyancy effects in rotating non-isothermal flows, in which the coexistence of the rotational forces and fluid temperature gradients leads to the emergence of rotation-induced buoyancy effects. Since the rotational forces are spatially varying with the local flow information, the buoyancy effects induced are obviously more sophisticated than the gravitational buoyancy resulted from constant gravity in a conventional natural/mixed convection flow. The coupling nature of the thermal flow phenomena with the rotational buoyancy is very influential to transport phenomena in the rotating system.

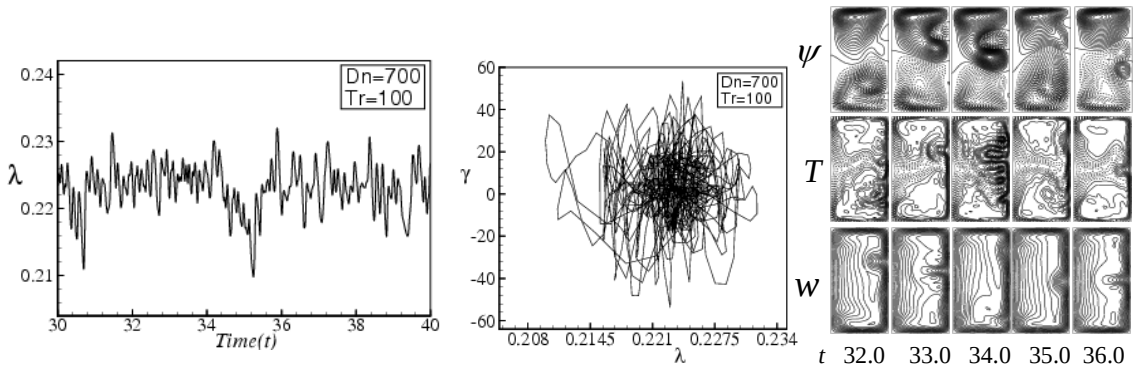

Figure 2. (a) Time evolution of λ for Dn = 700 and Tr = 100, (b) Phase space for Tr =100, (c) Contours of secondary flow patterns (top), temperature profiles (middle) and axial flow (bottom) for Tr = 100 at $32.0 \le t \le 36.0$.

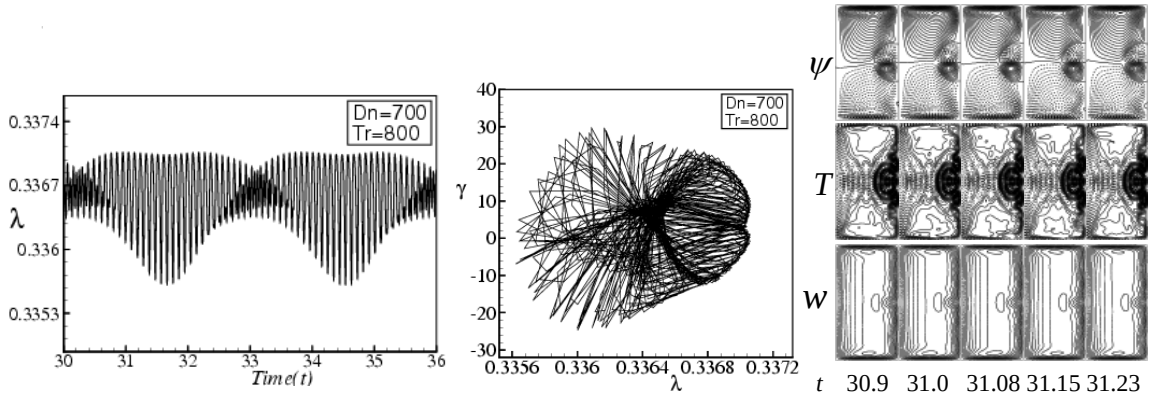

Figure 3. (a) Time evolution of λ for Dn = 700 and Tr = 800. (b) Phase space for Tr = 800, (c) Contours of secondary flow patterns (top), temperature profiles (middle) and axial flow distribution (bottom) for Tr = 800 at $30.93 \le t \le 31.23$

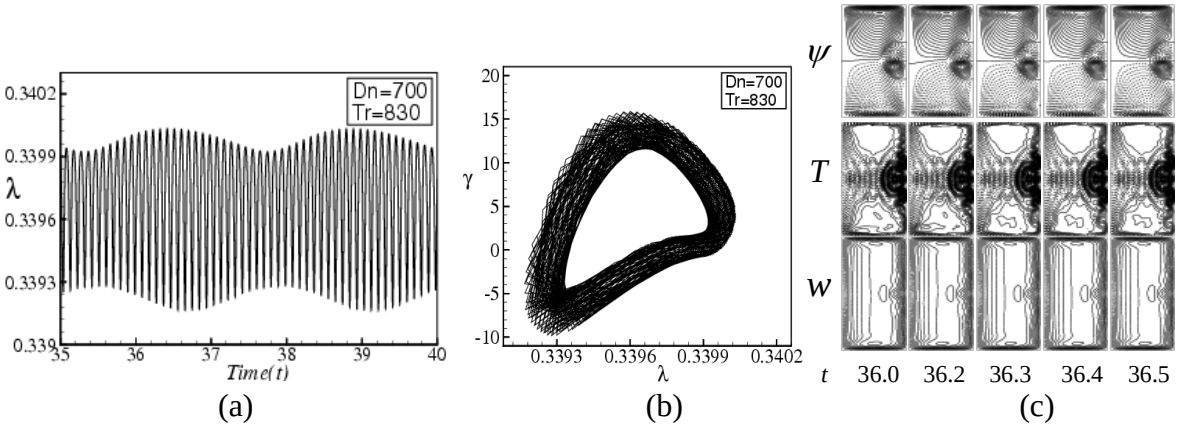

Figure 4. (a) Time evolution of λ for Dn = 700 and Tr = 830. (b) Phase space for Tr = 830, (c) Contours of secondary flow patterns (top), temperature profiles (middle) and axial flow distribution (bottom) for Tr = 830 at $36.0 \le t \le 36.5$

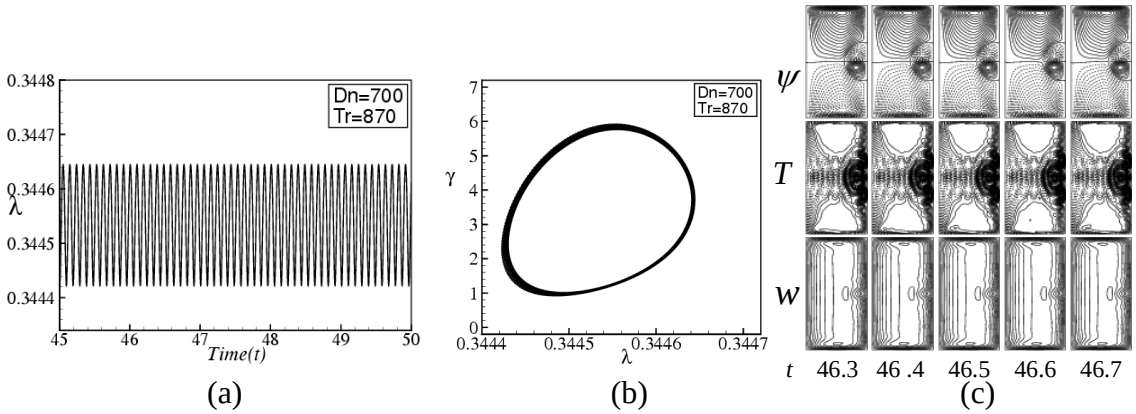

Figure 5. (a) Time evolution of λ for Dn = 700 and Tr = 870. (b) Phase space for Tr = 870, (c) Contours of secondary flow patterns (top), temperature profiles (middle) and axial flow (bottom) for Tr = 870 at $46.35 \le t \le 46.75$.

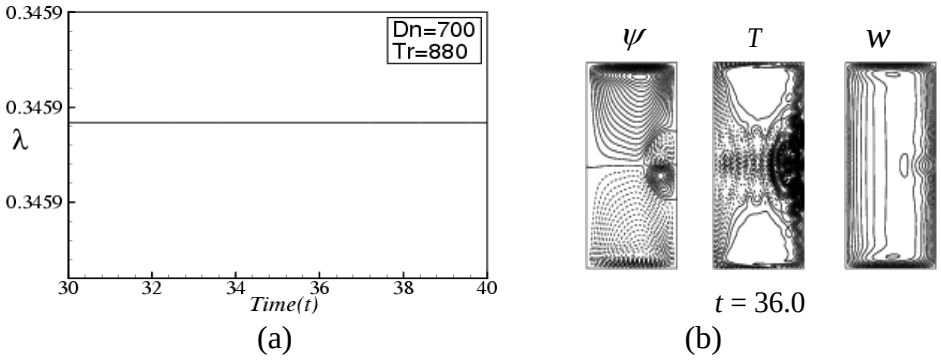

Figure 6. (a) Time evolution of λ for Dn = 700 and Tr = 880, (b) Contours of secondary flow patterns (left), temperature profiles (middle) and axial flow distribution (right) for Tr = 880 at $t = 36.0$.

Time evolution result for Tr = 870 is shown in Figure 5(a). It is found that the unsteady flow at Tr = 870 is a periodic solution whose orbit is single and it is well justified by drawing the phase space as shown in Figure 5(b). Contours of secondary flow patterns temperature profiles and axial flow distribution for the corresponding flow patterns are shown in Figure 5(c), where it is found that the periodic oscillation at Tr = 870 is a four-vortex solution. If the rotational speed is increased more in the positive direction, for example Tr = 880 up to 2000, it is found that the flow becomes steady state which is shown in Figure 6(a) for Tr = 880. Since the unsteady flow is a steady-state solution, single contours of secondary flow pattern, temperature profile and axial flow distribution is shown in Figure 6(b), and it is found that steady-state solution is a two-vortex flow.

6.2. *Case II*: Dean Number, *Dn* = 1000

Here, we performed time evolution of λ for $0 \le Tr \le 2000$ and $Dn = 1000$. Figure 7(a) shows time evolution of λ for $Tr = 500$. It is found that the unsteady flow at $Tr = 500$ is a strongly chaotic solution, which is well justified by drawing the phase spaces as shown in Figure 7(b). Figure 7(c) shows typical contours of secondary flow patterns, axial flow distribution and temperature profiles for $Tr = 500$, where we find that the unsteady flow is a six- and eight-vortex solution. Then we performed time evolution for $Tr = 1470$ as shown in Figure 8(a). It is found that the unsteady flow at $Tr = 1470$ is a multi-periodic solution which is well justified by depicting the phase space as shown in Figure 8(b). Contours of secondary flow patterns, temperature profiles and axial flow for the corresponding flow patterns has been shown in Figure 8(c) and where it is found that the multi-periodic oscillation at $Tr = 1470$ is a four-vortex solution. Continuing this process the time evolution for $Tr = 1485$ is displayed in Figure 9(a). It is observed that the unsteady flow at $Tr = 1485$ is a multi-periodic solution whose orbit is different and it is justified by drawing the phase space as shown in Figure 9(b).

Contours of secondary flow patterns, temperature profiles and axial flow for the corresponding flow patterns are expressed in Figure 9(c), where the four-vortex solution has been observed. Next, time evolution for $Tr = 1490$ is shown in Figure 10(a). It is found that the unsteady flow at $Tr = 1490$ is a periodic solution whose orbit is single and it is well justified by drawing the phase space as shown in Figure 10(b). Contours of secondary flow patterns temperature profiles and axial flow for the corresponding flow patterns are shown in Figure 10(c), where it is found that the periodic oscillation at $Tr = 1485$ is a four-vortex solution. Then, the rotational speed is increased more in the positive direction, for example $Tr = 1600$ up to 2000, and it is found that the flow becomes steady-state which is shown in Figure 11(a) for $Tr = 1600$. Since the unsteady flow is a steady-state solution, a single contour of secondary flow pattern, temperature profile and axial flow distribution is shown in Figure 11(b) and it is found that steady-state solution is an asymmetric two-vortex solution.

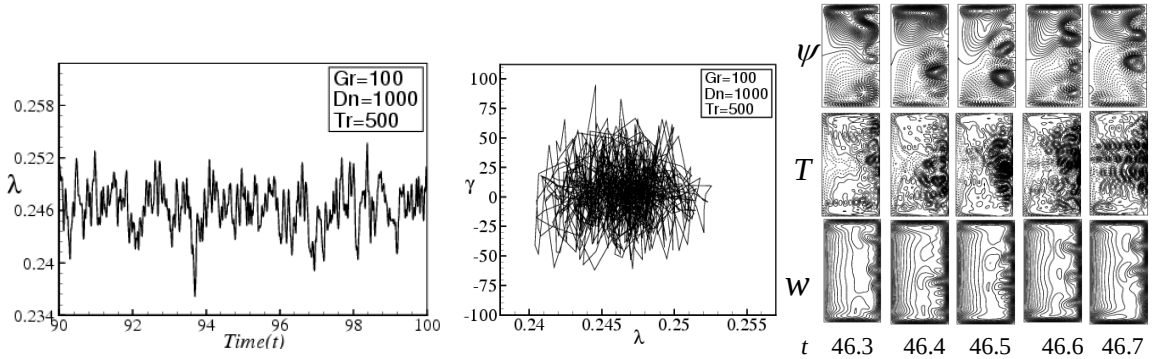

Figure 7. (a) Time evolution of λ for $Dn = 1000$ and $Tr = 500$. (b) Phase space for $Tr = 500$, (c) Contours of secondary flow patterns (top), temperature profiles (middle) and axial flow distribution (bottom) for $Tr = 500$ at $46.3 \le t \le 46.7$

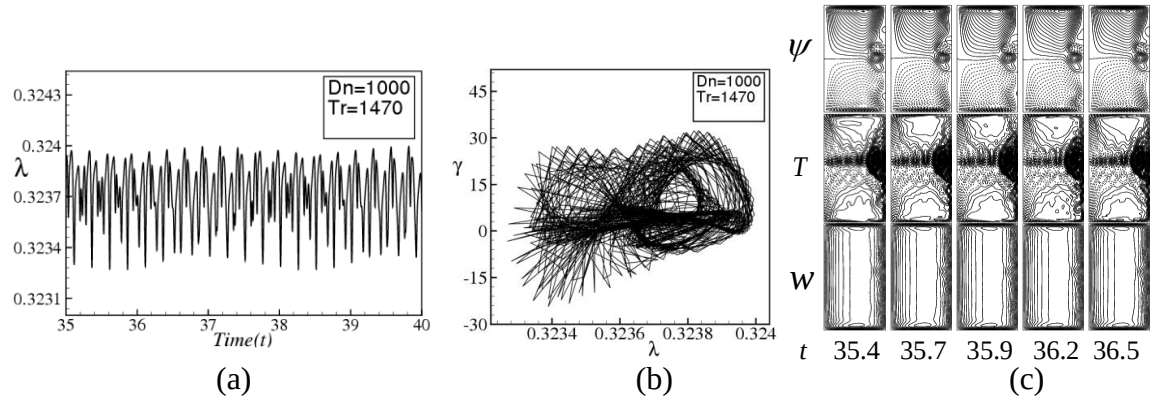

Figure 8. (a) Time evolution of λ for Dn = 1000 and Tr = 1470. (b) Phase space for Tr =1470, (c) Contours of secondary flow patterns (top), temperature profiles (middle) and axial flow distribution (bottom) for Tr = 1470 at $35.4 \le t \le 36.5$

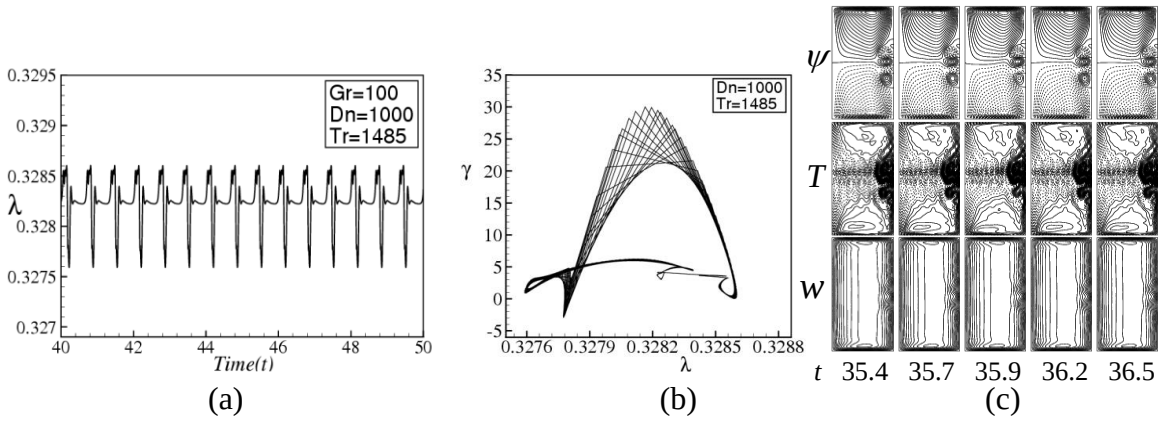

Figure 9. (a) Time evolution of λ for Dn = 1000 and Tr = 1490. (b) Phase space for Tr =1490, (c) Contours of secondary flow patterns (top), temperature profiles (middle) and axial flow (bottom) for Tr = 1490 at $35.4 \le t \le 36.5$

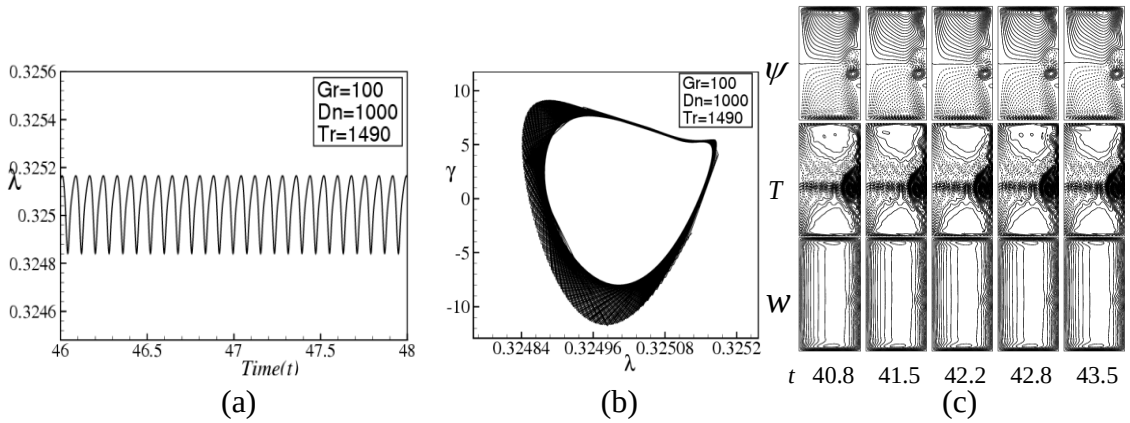

Figure 10. (a) Time evolution of λ for Dn = 1000 and Tr = 1490. (b) Phase space for Tr =1490, (c) Contours of secondary flow patterns (top), temperature profiles (middle) and axial flow (bottom) for Tr = 1490 at $40.8 \le t \le 43.5$.

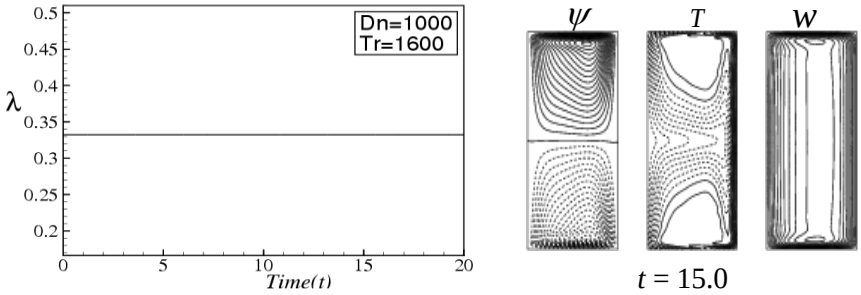

Figure 11. (a) Time evolution of λ for Dn = 1000 and Tr = 1600. (b) Phase space for Tr =1600, (c) Contours of secondary flow patterns (left), temperature profiles (middle) and axial flow (right) for Tr = 1600 at $t = 15.0$

7. CONCLUSION

A numerical study is presented for the flow characteristics through a rotating curved rectangular duct of aspect ratio 2.0 and curvature 0.1. Numerical calculations are carried out by using a spectral method and covering a wide range of the Taylor number $0 \le Tr \le 2000$ for the Dean numbers $100 \le Dn \le 1000$ and for the Grashof number Gr =100. We have investigated unsteady solutions for the positive rotation of the duct by time evolution calculations, and it is found that the unsteady flow undergoes in the scenario '*Chaotic → multi-periodic →periodic→ steady-state'*, if Tr is increased in the positive direction. In order to investigate the transition from multi-periodic oscillations to chaotic states more explicitly, the orbit of the solution is drawn in phase space. Drawing the phase spaces is found to be very fruitful to justify the transition of the unsteady flow characteristics as well as chaotic flow behavior. In this regard, it should be worth mentioning that irregular oscillation of the flow through a curved duct has been observed experimentally by Ligrani and Niver (1988) for a large aspect ratio and by Wang and Yang (2005) for the square duct. Typical contours of secondary flow patterns, temperature profiles and axial flow distribution are also obtained at several values of Tr, and it is found that there exist two-, four-, six- and eight-vortex solutions. The reason is that due to the combined action of the centrifugal-Coriolis-buoyancy force, we obtained two- to multi-vortex solution.

It is found that the temperature distribution is consistent with the secondary vortices and axial flow distributions, and convective heat transfer is significantly enhanced as the secondary vortices become stronger. The present study shows, there exists an asymmetric two-vortex solution for the steady-state solution, while asymmetric two-, three-, and four-vortex solutions for the periodic and multi-periodic solutions. For chaotic solution, on the other hand, we obtain asymmetric four-vortex solutions only. The present study also shows that chaotic flow enhances heat transfer more effectively than the steady-state or periodic solutions as the secondary flow become stronger for this case.

REFERENCES

Baylis, J. A., (1971). Experiments on Laminar Flow in Curved Channels of Square Section, Journal of Fluid Mechanics, Vol. 48(3), pp. 417-422.

Chandratilleke, T. T., Nadim, N. and Narayanaswamy, R., (2012). Vortex Structure-based Analysis of Laminar Flow Behavior and Thermal Characteristics in Curved Ducts, Int. J. Thermal Sciences, Vol. 59, pp. 75-86.

Dean, W. R., (1927). Note on the Motion of Fluid in a Curved Pipe, Philos. Mag., Vol. 4, pp. 208–223.

Guo, J., Xu, M., Cheng, L., (2011). Second Law Analysis of Curved Rectangular Channels, Int. J. Thermal Sciences, Vol. 50, pp.760-768.

Humphrey, J. A. C., Taylor, A. M. K. and Whitelaw, J. H., (1977). Laminar flow in a Square Duct of Strong Curvature, Journal of Fluid Mechanics, Vol. 83, pp. 509-527.

Islam, M. Z., Islam, M. S., & Islam, M. M, (2014). Pressure-Driven Flow Instability with Convective Heat Transfer through a Rotating Curved Channel with Rectangular Cross-Section: The Case of Negative Rotation, Journal of Mechanics of Continua and Mathematical Sciences, Vol. 9(1), pp. 1278-1291.

Ito, H. (1987). Flow in curved pipes. JSME International Journal, Vol. 30, pp. 543–552.

Kun, M. A, Yuan S., Chang, H. and Lai, H., (2014). Experimental Study of Pseudo plastic Fluid Flows in a Square Duct of Strong Curvature, Journal of Thermal Science, Vol. 23(4), pp. 359−367.

Ligrani, P. M. and Niver, R. D., (1988). Flow Visualization of Dean Vortices in a Curved Channel with 40 to I Aspect Ratio, Phys. Fluids, Vol. 31, pp. 3605-3617.

Mondal, R. N., Alam M. M. and Yanase, S. (2007). Numerical prediction of non- isothermal flows through a rotating curved duct with square cross section, Thommasat Int. J. Sci and Tech., Vol. 12, No. 3, pp. 24-43.

Mondal, R. N., Islam, M. Z., & Perven, R. (2014). Combined effects of centrifugal and coriolis instability of the flow through a rotating curved duct of small curvature. Procedia Engineering, Vol. 90, pp. 261-267.

Mondal, R. N., Datta, A. K. and Uddin, M. K. (2012). A Bifurcation Study of Laminar Thermal Flow through a Rotating Curved Duct with Square Cross-section, Int. J. Appl. Mech. and Engg., Vol. 17 (2).

Mondal, R. N., Islam, M. S., Uddin, M. K. and Hossain, M. A. (2013a). Effects of Aspect Ratio on Unsteady Solutions through a Curved Duct Flow, Appl. Math. & Mech., Vol. 34(9), pp.1-16

Mondal, R. N., Islam, M. Z. and Islam, M. S., (2013b). Transient Heat and Fluid Flow through a Rotating Curved Rectangular Duct: The Case of Positive and Negative Rotation, Procedia Engineering, Vol. 56, pp. 179-186.

Mondal, R. N., (2006). Isothermal and Non-isothermal Flows through Curved Duct with Square and Rectangular Cross-section, Ph.D. Thesis, Department of Mechanical Engineering, Okayama University, Japan.

Nandakumar, K. and Masliyah, J. H. (1986). Swirling Flow and Heat Transfer in Coiled and Twisted Pipes, Adv. Transport Process., Vol. 4, pp. 49-112.

Norouzi, M., Kayhani, M. H., Shu, C., and Nobari, M. R. H., (2010). Flow of Second-order Fluid in a Curved Duct with Square Cross-section, Journal of Non-Newtonian Fluid Mechanics, Vol. 165, pp. 323–339.

Norouzi, M. and Biglari, N., (2013). An Analytical Solution for Dean Flow in Curved Ducts with Rectangular Cross Section, Physics of Fluids, Vol. 25, 053602, pp. 1-15.

Selmi, M. and Namdakumar, K. (1999). Bifurcation Study of the Flow through Rotating Curved Ducts, Physics of Fluids, Vol. 11, pp. 2030-2043.

Selmi, M. and Namdakumar, K. and Finlay W. H., (1994). A bifurcation study of viscous flow through a rotating curved duct, Journal of Fluid Mechanics, Vol. 262, pp. 353-375.

Wang, L. and Yang, T., (2005). Periodic Oscillation in Curved Duct Flows, Physica D, Vol. 200, pp. 96-302.

Wang, L. Q. and Cheng, K.C., (1996). Flow Transitions and combined Free and Forced Convective Heat Transfer in Rotating Curved Channels: the Case of Positive Rotation, Physics of Fluids, Vol. 8, pp.1553-1573.

Wu, X. Y., Lai, S. D., Yamamoto, K., and Yanase, S. (2013). Numerical Analysis of the Flow in a Curved Duct, Advanced Materials Research, Vol. 706-708, pp. 1450-1453.

Yamamoto, K., Yanase, S. and Alam, M. M. (1999). Flow through a Rotating Curved Duct with Square Cross-section, J. Phys. Soc. Japan, Vol. 68, pp. 1173-1184.

Yanase, S., Kaga, Y. and Daikai, R. (2002). Laminar flow through a curved rectangular duct over a wide range of the aspect ratio, Fluid Dynamics Research, Vol. 31**,** pp. 151-183.